

# Low-energy excitations in the electron-doped metal phthalocyanine $\text{Li}_{0.5}\text{MnPc}$ from $^7\text{Li}$ and $^1\text{H}$ NMR

M. Filibian and P. Carretta

*Department of Physics "A.Volta," University of Pavia, Via Bassi 6, I-27100, Pavia, Italy*

T. Miyake, Y. Taguchi, and Y. Iwasa

*Institute for Materials Research, Tohoku University, Sendai 980-8577, Japan*

(Received 14 June 2006; revised manuscript received 7 September 2006; published 9 February 2007)

NMR and magnetization measurements in  $\text{Li}_{0.5}\text{MnPc}$  ( $\text{Pc} \equiv \text{C}_{32}\text{H}_{16}\text{N}_8$ ), recently proposed as a strongly correlated metal, are presented. Two different low-frequency dynamics are evidenced. The first one, probed by  $^1\text{H}$  nuclei, gives rise to a slowly relaxing magnetization at low temperature and is associated with the freezing of  $\text{MnPc}$   $S=3/2$  spins. This dynamics is similar to the one observed in pristine  $\beta\text{-MnPc}$  and originates from Li-depleted chain segments. The second one, evidenced by the  $^7\text{Li}$  spin-lattice relaxation rate, is associated with the hopping of the electrons along Li-rich chains. The characteristic correlation times for the two dynamics are derived, and the role of the disorder is briefly discussed.

DOI: 10.1103/PhysRevB.75.085107

PACS number(s): 71.27.+a, 76.60.Es, 75.50.Xx

## I. INTRODUCTION

Metal phthalocyanines (hereafter MPC) have attracted a lot of interest in the last decades owing to their technological applicabilities as dyes, gas sensors, or in electro-optical devices.<sup>1</sup> A renewed interest on these systems has emerged after the observation that thin films of MPC show a marked increase in the electrical conductivity once they are doped with alkali ions.<sup>2</sup> In view of the similarities that alkali-doped MPC ( $A_x\text{MnPc}$ ) share with fullerenes, Tosatti *et al.*<sup>3</sup> have considered the possibility that superconductivity could occur also in  $A_x\text{MnPc}$ . Within a model successfully applied to other strongly correlated electron systems,<sup>4</sup> they found that strongly correlated superconductivity could develop in  $A_x\text{MnPc}$  for  $x \approx 2$ , with a magnitude and a symmetry of the order parameter which would depend on the intensity of the local exchange (Hund coupling) and Jahn-Teller couplings.<sup>3</sup> Accordingly a growing interest in these compounds has arisen in the last year. Nevertheless, the synthesis of bulk  $A_x\text{MnPc}$  is nontrivial and hitherto still at a preliminary stage. So far only  $\beta\text{-Li}_x\text{MnPc}$  powders have been grown in a reproducible way, for  $0 \leq x \leq 4$ ,<sup>5</sup> and the evolution of the lattice parameters and of the basic magnetic properties with doping have been studied.

$\text{Li}_x\text{MnPc}$  structure (Fig. 1) is formed by chains along which  $\text{MnPc}$  molecules are stacked. From high-resolution x-ray diffraction it was observed that  $\text{Li}^+$  ions stay in between adjacent  $\text{MnPc}$  molecules and are tightly bound to pyrrole-bridging N atoms.<sup>5</sup> This one-dimensional structure is similar to the one of other organic conductors which have been deeply investigated in the last 20 years and are still subject of an intense research activity: the Bechgaard salts.<sup>6</sup> Magnetization measurements carried out in  $\text{Li}_x\text{MnPc}$  have revealed a progressive increase in the Curie constant with doping and a modification in the magnitude and sign of the superexchange coupling, a neat demonstration that electrons are transferred to  $\text{MnPc}$  molecular orbitals. In order to study the modifications of the microscopic electronic properties of  $\text{Li}_x\text{MnPc}$  with doping, one can conveniently use local probes

as  $^7\text{Li}$  and  $^1\text{H}$  nuclei. In the following we present a  $^7\text{Li}$  and  $^1\text{H}$  nuclear magnetic resonance (NMR) and magnetization study of  $\text{Li}_{0.5}\text{MnPc}$ . From nuclear spin-lattice relaxation measurements two different dynamics were found: a low-frequency dynamics associated with the progressive freezing of  $\text{MnPc}$   $S=3/2$  spins and a dynamics at much higher frequency of diffusive character. The characteristic correlation times of these dynamics, the hyperfine couplings, and the temperature and time evolution of the macroscopic magnetization are estimated and discussed in the light of the possible evolution of the molecular electronic and spin configuration. The experimental results are presented in the following section. Section III is dedicated to their analysis and discussion, while the final conclusions are presented in Sec. IV.

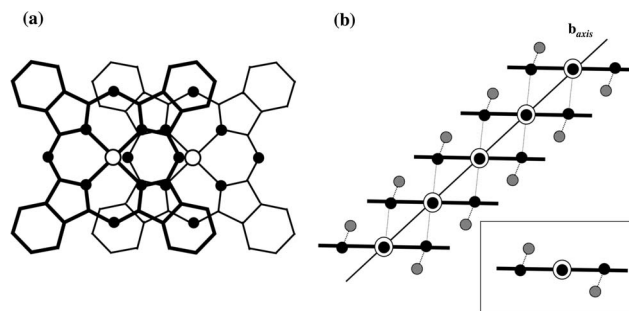


FIG. 1. (a) Projection of two neighboring  $\text{MnPc}$  molecules within the same stack along the direction normal to the planar rings, in  $\text{Li}_2\text{MnPc}$ . The  $\text{Mn}^{2+}$  ions are depicted as open circles lying directly above (below) neighboring (black solid circles) N atoms. (b) The slip-stacked  $\text{MnPc}$  assembly along the  $b$  axis in  $\text{Li}_2\text{MnPc}$ .  $\text{Li}^+$  ions (depicted in gray) are disordered and reside exclusively in the intrastack spacing and bond strongly to pyrrole-bridging N atoms (dotted lines). The inset shows the  $\text{Li}_2\text{MnPc}$  building block of the 1D assemblies.

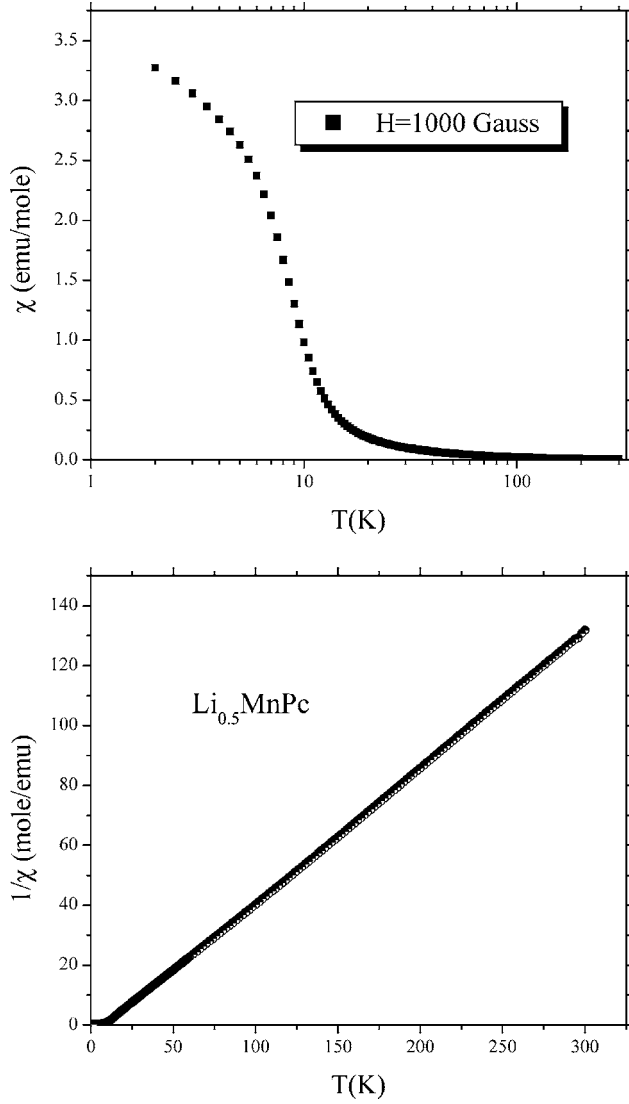


FIG. 2. (Top) Temperature dependence of the susceptibility, defined as  $\chi = M/H$ , in  $\text{Li}_{0.5}\text{MnPc}$  for  $H = 1$  kG. (Bottom) Temperature dependence of the inverse of the susceptibility. One can notice that for  $T \geq 15$  K the Curie-Weiss law is obeyed.

## II. TECHNICAL ASPECTS AND EXPERIMENTAL RESULTS

As-purchased MnPc powder was purified by vacuum sublimation prior to the intercalation procedure. Li intercalation was carried out by using a liquid-phase process in an Ar-filled glove box. Details on these procedures are described in Ref. 5. The powder samples were sealed in a quartz tube to avoid oxidation.

Magnetization measurements were performed using a Quantum Design XPMS-XL7 superconducting quantum interference device (SQUID) magnetometer. At high temperatures, above 15 K, the magnetization  $M$  was found to increase linearly with the field  $H$  and the susceptibility is given by  $\chi = M/H$ . One observes (Fig. 2) a high-temperature Curie-Weiss behavior

$$\chi = \frac{C}{T - \Theta} + \chi_0, \quad (1)$$

with  $C = 2.27$  emu K/mol Curie constant and  $\Theta = 7.5 \pm 0.1$  K, indicating a dominant ferromagnetic coupling.  $\chi_0$  is the sum of Van Vleck and diamagnetic contributions, which are assumed weakly temperature dependent.<sup>7</sup> Below about 10 K a clear departure from the Curie-Weiss law is observed (Fig. 2). The magnetization shows an upturn, is no longer linear in field, and is observed to slowly relax in time, suggesting a freezing of the molecular spins. This behavior is reminiscent of the one observed in pure  $\beta$ -MnPc.<sup>5</sup>

NMR measurements were performed by using standard radio-frequency (rf) pulse sequences.  $^7\text{Li}$  and  $^1\text{H}$  powder spectra were obtained from the Fourier transform of half of the echo signal after a  $\pi/2 - \tau - \pi/2$  pulse sequence. The spectra were observed to be Gaussian with a linewidth increasing upon cooling, as the macroscopic susceptibility. In  $^7\text{Li}$  ( $I = 3/2$ ) spectra there was no clear evidence of the satellite transitions, which are much less intense than the central one, even though we observed that the length of the  $\pi/2$  pulse was about half of that derived for  $^7\text{Li}$  in an aqueous solution of LiCl, where all transitions are irradiated. This indicates that practically just  $^7\text{Li}$  central ( $m_I = 1/2 \leftrightarrow -1/2$ ) line was irradiated. The echo intensity  $E(2\tau)$  was observed to decay with  $\tau$  following a nearly Gaussian law, with a characteristic decay time  $T_2^G = 165 \pm 10 \mu\text{s}$  for  $^7\text{Li}$  and  $T_2^G = 45 \pm 3 \mu\text{s}$  for  $^1\text{H}$ , around 100 K. Finally, the relative intensity of  $^7\text{Li}$  and  $^1\text{H}$  signals for  $\tau \rightarrow 0$  was observed to be consistent with a Li content of  $0.50 \pm 0.01$  per formula unit, in excellent agreement with the expected nominal doping.

The nuclear spin-lattice relaxation rate  $1/T_1$  was estimated from the recovery of nuclear magnetization  $m(\tau)$  after a saturating rf pulse sequence. The  $^7\text{Li}$  recovery law was observed to be a stretched exponential (Fig. 3): namely,  $y(\tau) \equiv 1 - m(\tau)/m(\tau \rightarrow \infty) = \exp[-(\tau/T_1)^\beta]$ , with  $\beta \approx 0.45$  over the whole temperature range (Fig. 4). Also the  $^1\text{H}$  recovery law was essentially of stretched exponential character; however, for large delays  $\tau$  a clear departure from a simple stretched exponential recovery was noticed. The recovery could be nicely fit according to (Fig. 5)

$$y(\tau) = A e^{-(\tau/T_1^A)^\beta} + (1 - A) e^{-(\tau/T_1^B)}, \quad (2)$$

with  $A \approx 0.8$  and  $\beta \approx 0.5$  over the explored temperature range (Fig. 4). This indicates that two distinct  $^1\text{H}$  relaxation processes are present.

The observed stretched exponential recoveries indicate a distribution of relaxation rates  $1/T_1^i$ , with an average relaxation  $1/T_1^A$  given by<sup>8</sup>

$$1/T_1^A = \int f(1/T_1^i) 1/T_1^i di, \quad (3)$$

where  $f(1/T_1^i)$  is a distribution function. For  $f(1/T_1^i) \equiv \delta(1/T_1^i - 1/T_1^A) \equiv \delta(1/T_1^i - 1/T_1)$  (i.e., the same relaxation rate for all nuclei), one has clearly a simple exponential decay ( $\beta = 1$ ). On the other hand, the recovery law  $y(\tau) = e^{-(\tau/T_1^A)^{1/2}}$ , close to the one found for  $^7\text{Li}$  and for the

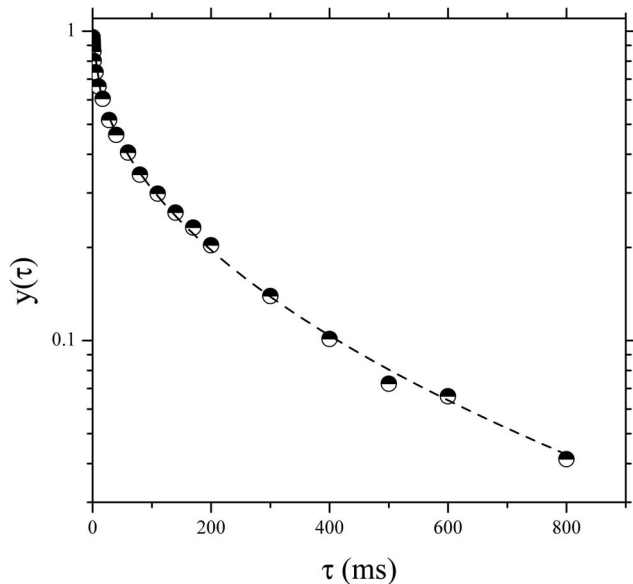


FIG. 3. Recovery law for <sup>7</sup>Li nuclear magnetization after a saturating pulse sequence. The dashed line is the best fit according to  $y(\tau) = \exp[-(\tau/T_1)^\beta]$ .

fast component of <sup>1</sup>H, is expected when  $f(1/T_1^i) \equiv \sqrt{1/T_1^A} / 2\sqrt{\pi(1/T_1^i)^3 \exp[-(1/T_1^A)/(4(1/T_1^i))]}$ .<sup>8</sup> Therefore, the measured  $1/T_1$  is close to  $1/T_1^A$ , the average relaxation rate. While in general  $f(1/T_1^i)$  can be significantly temperature dependent, our data rather show that in  $\text{Li}_{0.5}\text{MnPc}$ ,  $\beta$ , and then  $f(1/T_1^i)$ , changes very slightly with temperature.

The temperature dependence of the <sup>7</sup>Li and <sup>1</sup>H relaxation rates derived from the aforementioned recovery laws are shown in Figs. 6 and 7. At temperatures above 35 K, the <sup>1</sup>H relaxation rate  $1/T_1^s$  shows a low-frequency divergence with  $1/T_1^s \propto 1/\sqrt{H}$  (Fig. 8), a behavior which is observed also in

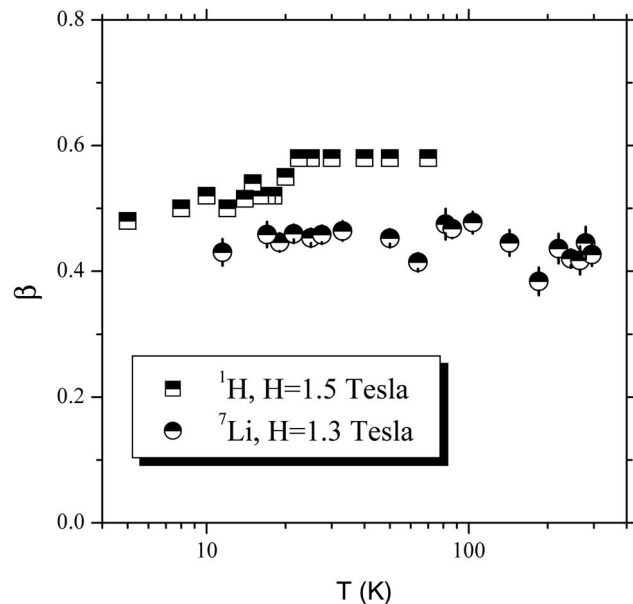


FIG. 4. Temperature dependence of the stretched exponential exponent  $\beta$  for <sup>7</sup>Li and for the fast component of <sup>1</sup>H recovery laws.

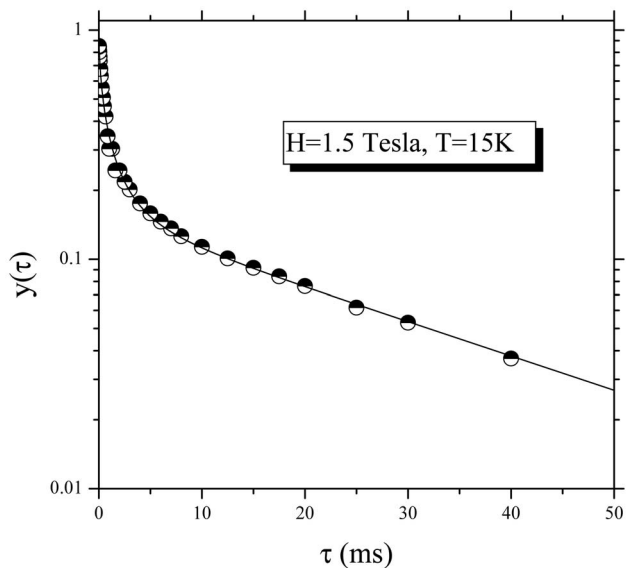


FIG. 5. Recovery law for <sup>1</sup>H nuclear magnetization after a saturating pulse sequence. The solid line is the best fit according to Eq. (2).

other MPc (Ref. 9) and, in general, is typical of one-dimensional spin systems.<sup>10</sup>

### III. DISCUSSION

The temperature dependence of the magnetic susceptibility is characteristic of ferromagnetically correlated spin chains, as observed for pristine  $\beta$ -MnPc. The fit of the susceptibility according to the Curie-Weiss law yields  $\Theta = 7.5 \pm 0.1$  K, corresponding to an exchange coupling constant  $J = 3\Theta/[2zS(S+1)] = 1.5 \pm 0.02$  K, for  $S = 3/2$  and taking  $z = 2$  for the number of nearest neighbors. This value of  $\Theta$  is

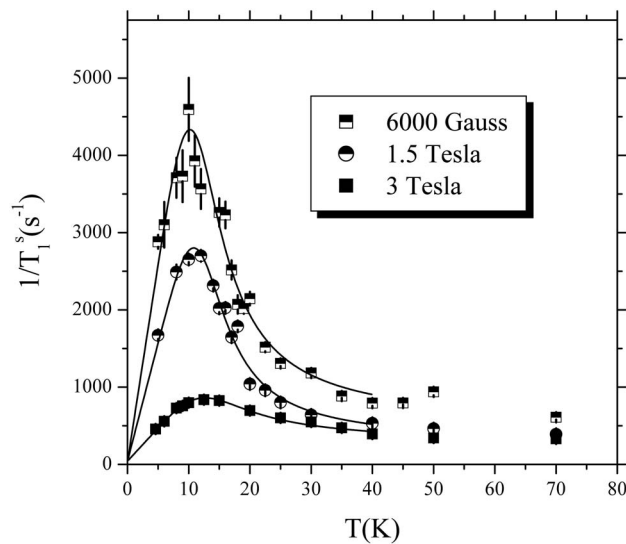


FIG. 6. Temperature dependence of <sup>1</sup>H  $1/T_1^s$  at different magnetic fields. The solid lines are the best fit according to Eq. (9), for  $\langle E_A \rangle = \Delta = 25 \pm 5$  K.

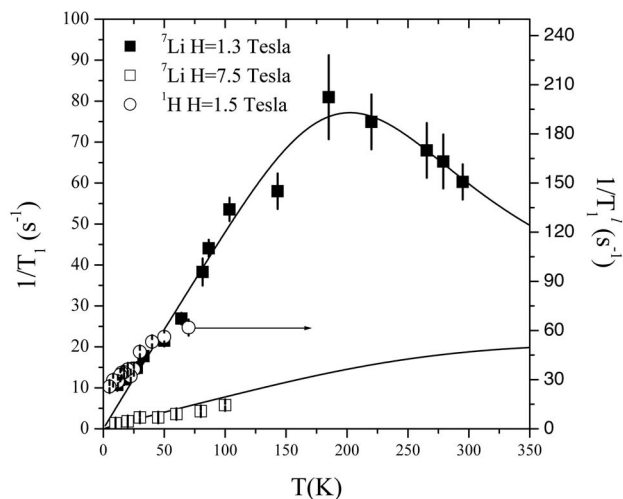


FIG. 7. Temperature dependence of  ${}^7\text{Li}$   $1/T_1$  (squares) and of  ${}^1\text{H}$   $1/T_1^l$  (circles and right vertical scale), the relaxation rate of the slowly relaxing component of  ${}^1\text{H}$  magnetization (see Fig. 5). The solid lines are the best fit according to Eq. (9), for  $\langle E_g \rangle = \Delta = 410 \pm 46$  K.

lower than the one of pure  $\beta\text{-MnPc}$ , whereas the Curie constant is larger in  $\text{Li}_{0.5}\text{MnPc}$ , in agreement with the results reported by Taguchi *et al.*<sup>5</sup> for  $0 \leq x \leq 4$ . In fact, they observed that for  $x \rightarrow 2$  Curie constant tends to the one expected for  $S=5/2$  with  $g=2$ , while  $\Theta$  becomes negative; i.e., the chain becomes antiferromagnetically correlated.

$\beta\text{-MnPc}$  in its ground state has a completely filled  $a_{1u}$  level, a half-filled  $a_{1g}$  level, and two degenerate half-filled  $1e_g$  levels.<sup>7,11</sup> In order to attain an  $S=5/2$  molecular spin state upon increasing Li content, it is necessary to start filling the upper energy levels, as the twofold-degenerate  $2e_g(\pi)$  lowest unoccupied molecular orbital (LUMO) and the  $b_1(d_{x^2-y^2})$

states, a scenario which differs from the one of  $\text{MPC}$  containing transition metal ions with more  $d$  electrons than  $\text{Mn}^{2+}$ . In fact, in  $\text{FePc}$  and  $\text{CoPc}$  the Hund rule is not obeyed and the other electrons occupy the  $1e_g$  levels, so that one has an  $S=1$  and an  $S=1/2$  configuration, respectively. Taking into account the crystal-field modifications induced by  $\text{Li}^+$ , the  $S=5/2$  state could in principle result from two different configurations. As suggested in Ref. 5,  $\text{Li}^+$  gives rise to a more isotropic crystal field and the energy of the LUMO and  $b_1(d_{x^2-y^2})$  can be lowered, so that an electron can be promoted from the  $a_{1u}$  to the  $b_1(d_{x^2-y^2})$  level, in accordance with Hund's rule. Then the  $S=5/2$  state would result from the occupancy of all  $d$ -character orbitals. The electrons injected by Li doping, which fill the  $2e_g(\pi)$  LUMO, would not contribute to the total molecular spin once they form a singlet state, a situation similar to the one observed in the fullerenes.<sup>12</sup> Singlet formation can occur if Jahn-Teller coupling for the  $2e_g(\pi)$  state with the  $B_{1g}$  and  $B_{2g}$   $\beta\text{-MnPc}$  vibrational modes is larger than its Hund coupling.<sup>3</sup>

On the other hand, an  $S=5/2$  state is also consistent with a triplet state for the electrons on the LUMO, provided that the  $b_1(d_{x^2-y^2})$  energy is not significantly lowered by Li doping and this latter level remains empty. The comprehension of which one of the two configurations is actually taking place is important, as it will allow one to know which one of the two couplings, Jahn-Teller or Hund's, is dominant for the electrons on the LUMO. Nevertheless, from our measurements alone it is not possible to discern among the two scenarios. Crystal-field calculations and microscopic techniques using  $\text{Mn}^{2+}$  ions as probes [e.g., electron paramagnetic resonance (EPR)] would allow one to clarify this aspect. It is noticed that the filling of the LUMO, which overlaps with the  $a_{1g}$  orbitals of adjacent molecules along the chain, can induce antiferromagnetic correlations,<sup>13</sup> which would explain the change of sign of Curie-Weiss temperature with increasing doping.

The configuration with two  $\text{Li}^+$  ions close to an  $\text{MnPc}$  molecule gives rise to a crystal field which decreases the energy of the  $b_1$  states and also of the LUMO. Accordingly, one should expect that the energy of  $S=5/2$  state is possibly lower than the one of  $S=2$  and  $S=3$  states, associated with one unpaired electron on the LUMO. Then, it is likely that the progressive increase in the Curie constant, upon increasing Li content from  $x=0$  to 2, actually originates from the contribution of  $S=3/2$  and of  $S=5/2$  chain segments, which are characterized by a more stable spin configuration. Although from magnetization data alone one cannot say if both spin configurations coexist at the microscopic level, we remark that  $\text{Li}_x\text{MnPc}$  susceptibility data can be fit with  $\chi = (x/2)\chi_{\text{Li}_2} + [(2-x)/2]\chi_{\text{Li}_0}$ , for  $T \gg 10$  K, where the  $\chi_{\text{Li}_{x=0,2}}$  susceptibilities are the ones derived by Taguchi *et al.*<sup>5</sup> for  $x=0$  and  $x=2$ . As will be pointed out later on, this interpretation is corroborated by the observation of two different dynamics in nuclear spin-lattice relaxation measurements.

The deviation from Curie-Weiss law observed at low temperature is not associated with a three-dimensional long-range order. In fact, below 10 K one observes a slowly relaxing magnetization which indicates a progressive freezing of the molecular spins, a scenario observed in other spin

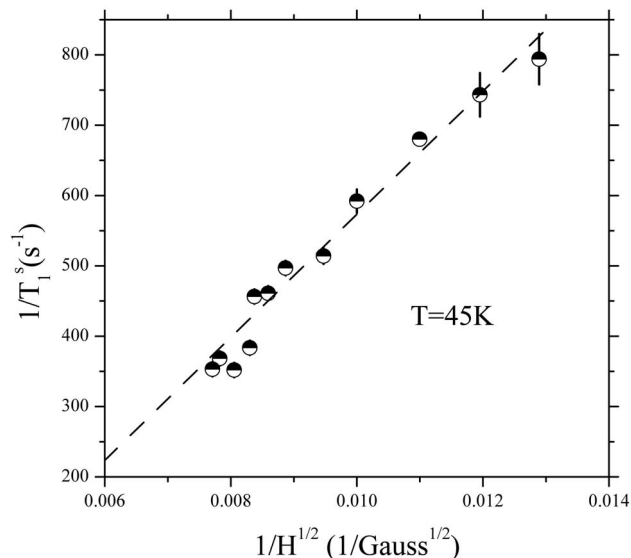


FIG. 8.  ${}^1\text{H}$  nuclear spin-lattice relaxation rate  $1/T_1^s$ , at  $T=45$  K, reported as a function of  $1/\sqrt{H}$  in order to evidence the diffusive nature of the spin correlations. The dashed line is the best fit according to Eq. (7) in the text.

chains characterized by a sizable magnetic anisotropy.<sup>14</sup> At a temperature of 3 K the magnetization was observed to relax in a characteristic time  $\tau_M = 1050 \pm 90$  s upon increasing the field from 0 to 1 T. This relaxation time is comparable with the average relaxation time measured by means of ac susceptibility.<sup>5</sup> In fact, from the peak in the imaginary part of the ac susceptibility measured at different frequencies one can roughly estimate an average correlation time  $\tau_{ac} \approx 10^{-10} \exp(90/T)$  s, corresponding to  $\tau_{ac} \approx 1070$  s at 3 K, in rather good agreement with the value estimated from the relaxation of the magnetization.

Now we turn to the analysis of the low-energy excitations in the light of nuclear spin-lattice relaxation rate  $1/T_1$  measurements. In the presence of a magnetic relaxation mechanism,

$$\frac{1}{T_1} = \frac{\gamma^2}{2} \int_{-\infty}^{+\infty} e^{i\omega_N t} \langle h_+(t) h_-(0) \rangle dt, \quad (4)$$

where  $h_{\pm}$  are the transverse components of the hyperfine field at the nucleus,  $\omega_N$  the nuclear resonance frequency, and  $\gamma$  the nuclear gyromagnetic ratio. In MPC, spin-lattice relaxation processes originate from the hyperfine coupling between nuclear and molecular spins. Therefore one can write  $\tilde{h}(t) = \sum_i \tilde{A}_i \tilde{S}_i(t)$ , with  $\tilde{A}_i$  the hyperfine coupling between the  $i$ th spin, and then  $1/T_1$  probes the electron spin-spin correlation functions  $g_j^\alpha(t) = \langle S_i^\alpha(t) S_{i+j}^\alpha(0) \rangle$  ( $\alpha = x, y, z$  and  $i$  and  $j$  are site indices), which decay in a characteristic correlation time  $\tau_c$ .

The  $T_1$  distribution evidenced by the stretched exponential recovery of nuclear magnetization could arise either from different hyperfine couplings or from a distribution of correlation times for the spin fluctuations. Indeed, in the Pc molecule there are nonequivalent  $^1\text{H}$  sites; however, as will be shown later on [see Eq. (9)], in order to explain the experimental data it is necessary to invoke also a distribution of correlation times. Such a distribution could originate from the local disorder, as the one associated with alternating Li-rich and Li-depleted chain segments.

In a single crystal the magnitude of the hyperfine coupling can be estimated from the shift of the resonance frequency  $\omega_N$  with respect to the nuclear Larmor frequency  $\omega_0$  in an applied magnetic field. In fact, one can write

$$\frac{\omega_N - \omega_0}{\omega_0} \equiv \Delta\tilde{K} = \frac{\tilde{A}\tilde{\chi}}{g\mu_B N_A}, \quad (5)$$

where the macroscopic susceptibility  $\tilde{\chi}$ , the hyperfine coupling  $\tilde{A} = \sum_i \tilde{A}_i$ , and the shift  $\Delta\tilde{K}$  are all tensors, in principle. Therefore, in a powder one should observe an effective broadening of the line rather than a shift. Indeed both for  $^1\text{H}$  and  $^7\text{Li}$  one observes that the line broadens with increasing  $\chi$  (Figs. 9 and 10). The line shape is Gaussian for both nuclei, and no structure associated with the form of the shift tensor can be discerned. By plotting the line broadening  $\Delta\omega$  vs  $\chi$ , with the temperature as an implicit parameter, one can estimate an effective coupling constant  $A$ . For both nuclei one finds  $A \approx 100$  G, which is of the order of magnitude of the

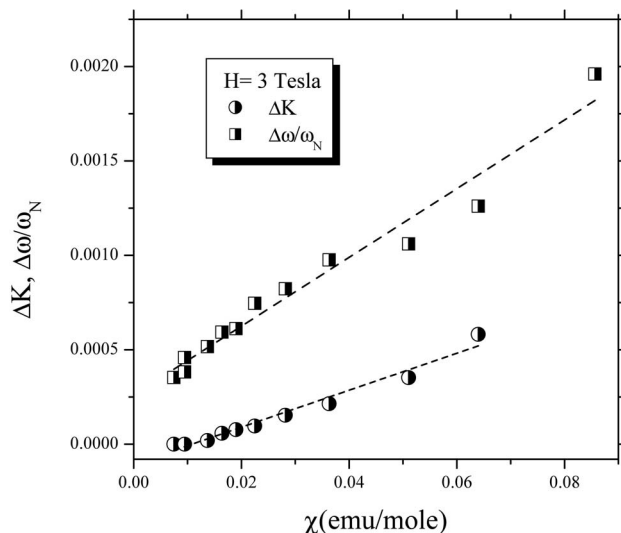


FIG. 9.  $^1\text{H}$  paramagnetic shift  $\Delta K$  [see Eq. (5)] and normalized line broadening  $\Delta\omega/\omega_N$  reported as a function of the magnetic susceptibility measured with the SQUID magnetometer, with the temperature as an implicit parameter. The dashed lines evidence the linear dependence of the line broadening and of the shift on the susceptibility [see Eq. (5)].

dipolar hyperfine field generated by localized electron spins. It is noticed that  $^1\text{H}$  spectra also show a slight shift on cooling (Fig. 9), still proportional to  $\chi$  and yielding an isotropic hyperfine coupling constant around 100 G.

In the high-temperature limit  $T \gg J$  the spins are uncorrelated and, in the absence of diffusive processes, one would expect a temperature- and field-independent  $1/T_1$ , with<sup>10</sup>

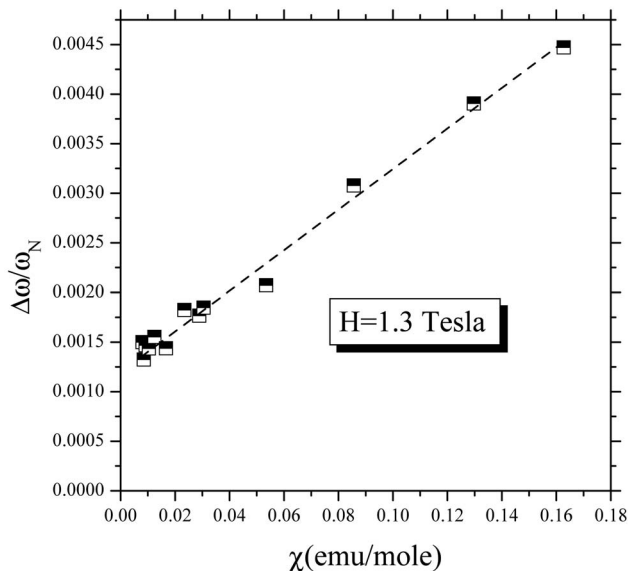


FIG. 10.  $^7\text{Li}$  normalized line broadening  $\Delta\omega/\omega_N$  reported as a function of the magnetic susceptibility measured with the SQUID magnetometer, with the temperature as an implicit parameter.

$$\left(\frac{1}{T_1}\right)_{T \gg J} = \gamma^2 A^2 \frac{S(S+1)}{3} \frac{\sqrt{2\pi}}{\omega_H}, \quad (6)$$

where  $\omega_H = (2zJ/k_B)\sqrt{S(S+1)}/3$  is the Heisenberg exchange frequency. Indeed, above 40 K, one observes that  ${}^1\text{H}$   $1/T_1^s$  is practically temperature independent. However, on the basis of Eq. (6) one would estimate  $1/T_1^s$  around  $23 \text{ s}^{-1}$  at least an order of magnitude lower than the experimental value (Fig. 6); moreover,  $1/T_1^s$  is strongly field dependent (Fig. 8), at variance with what Eq. (6) predicts. The marked field dependence of  $1/T_1^s$  for  $T \gg J$  can be associated with the diffusive character of the spin correlations, which in one dimension gives rise to a  $1/\sqrt{H}$  low-frequency divergence in the spectral density.<sup>9,10</sup> In fact, by neglecting low-frequency cutoffs,<sup>10</sup> one has

$$\left(\frac{1}{T_1}\right)_{T \gg J} = \gamma^2 A^2 \frac{S(S+1)}{3} \frac{1}{\sqrt{2D}} \frac{1}{\sqrt{\omega_N}}. \quad (7)$$

By fitting the data in Fig. 8 with the above equation one estimates a diffusion constant  $D \approx (1.2 \pm 0.1)\omega_H$ , of the right order of magnitude. This diffusive dynamic has been also observed in an early work on CuPc.<sup>9</sup>

It is noticed that upon cooling below 20 K,  $1/T_1^s$  rapidly increases and then shows a broad maximum around 10 K. The amplitude of the maximum is strongly field dependent and is not associated with a three-dimensional ordering, but rather signals dynamics at frequencies of the order of  $\omega_N \ll \omega_H$ . This maximum should not be confused with the one due to soliton excitations observed in some one-dimensional ferromagnets for  $T \ll J$ , which would cause a completely different magnetic field dependence of  $1/T_1$ .<sup>15</sup> This low-frequency dynamic should rather be ascribed to the progressive freezing of the molecular spins, as detected by means of ac susceptibility in pristine  $\beta$ -MnPc.<sup>5</sup> It should be remarked that a slowing down of the frequency of the spin fluctuations to the MHz range at  $T > \Theta$  can occur only if the magnetic anisotropy barrier  $E_A = DS_z^2 \geq \Theta$  and overcomes the thermal energy  $k_B T$ . This situation is analogous to the one observed in single-molecule magnetic clusters<sup>16</sup> and has also been observed in  $\alpha$ -FePc.<sup>13</sup> Thus, one should distinguish two regimes: a high-temperature one ( $k_B T > E_A$ ) where Eq. (7) applies and a low-temperature one ( $k_B T < E_A$ ) characterized by a very low-frequency activated dynamic.

Now, if one assumes that the correlation function describing the low-frequency dynamic  $\langle h_+(t)h_-(0) \rangle = \langle \Delta h_\perp^2 \rangle \times \exp(-t/\tau_c)$ , with  $\langle \Delta h_\perp^2 \rangle \approx 2A^2 S(S+1)/3$ , from Eq. (4) one derives

$$\frac{1}{T_1} = \frac{\gamma^2 \langle \Delta h_\perp^2 \rangle}{2} \frac{2\tau_c}{1 + \omega_N^2 \tau_c^2}. \quad (8)$$

Taking into account that the molecular anisotropy yields an effective energy barrier  $E_A$ , one can write  $\tau_c = \tau_0 \exp(E_A/T)$  ( $E_A$  in kelvin). If we try to fit  ${}^1\text{H}$   $1/T_1^s$  data by taking this expression for  $\tau_c$  in Eq. (8), a poor fit is obtained. In fact, the

broad maximum in  $1/T_1^s$  indicates a distribution of correlation times generated by a distribution of activation energies. In light of Eq. (3), if we consider a rectangular distribution  $p(E_A)$  of activation energies from  $\langle E_A \rangle - \Delta$  to  $\langle E_A \rangle + \Delta$ , then the average relaxation time turns out to be<sup>17</sup>

$$\begin{aligned} \left(\frac{1}{T_1}\right)_A &= \int_{-\Delta}^{+\Delta} p(E_A) 1/T_1(E_A) dE_A \\ &= \frac{\gamma^2 \langle \Delta h_\perp^2 \rangle T}{2 \omega_N \Delta} \left[ \arctan(\omega_N \tau_0 e^{\langle E_A \rangle + \Delta/T}) \right. \\ &\quad \left. - \arctan(\omega_N \tau_0 e^{\langle E_A \rangle - \Delta/T}) \right]. \end{aligned} \quad (9)$$

A good fit of  $1/T_1^s$  data for  $T \leq 40$  K is obtained for  $\tau_0 = (1 \pm 0.4) \times 10^{-10}$  s and  $\langle E_A \rangle = \Delta = 25 \pm 5 \text{ K} > \Theta$ , as expected for a freezing of MnPc spins. It should be remarked that this activation energy is quite different from the one (about 90 K) derived from the analysis of ac susceptibility data. Since  $1/T_1$  probes the  $q$ -integrated spin susceptibility,<sup>18</sup> while the ac susceptibility the  $\vec{q}=0$  modes, this observation would indicate a more rapid softening of the latter ones with respect to the other  $\vec{q}$  modes, as expected for a dominant ferromagnetic character of the spin correlations.

Now we turn to the discussion of  ${}^7\text{Li}$   $1/T_1$ . If one considers that the order of magnitude of the hyperfine coupling of  ${}^7\text{Li}$ , derived from the line broadening (Fig. 10), is the same as  ${}^1\text{H}$ , one would expect also a peak in  ${}^7\text{Li}$   $1/T_1$  around 10 K. Remarkably,  ${}^7\text{Li}$   $1/T_1$  does not show any peak; it decreases upon cooling and is much smaller than  $1/T_1^s$  (see Figs. 6 and 7). The absence of a low-temperature peak in  ${}^7\text{Li}$   $1/T_1$  cannot be due to a filtering of the spin excitations at the critical wave vector, as Li is not in a symmetric position with respect to Mn ions<sup>18</sup>; moreover,  $1/T_1$  starts decreasing at  $T \gg J$ . Now, the  ${}^7\text{Li}$   $1/T_1$  temperature dependence is clearly similar to the one observed for  $1/T_1^l$ , the slowly relaxing component of  ${}^1\text{H}$  magnetization. This analogy suggests that Li insertion deeply affects the local spin dynamics so that neighboring protons do not probe the low-temperature Mn freezing. As discussed before, it is likely that the two microscopic configurations with either zero or two Li atoms per molecule are the most favored in  $\text{Li}_{0.5}\text{MnPc}$ , which is effectively composed of alternated chain segments. In Li-rich segments, in particular, the modification of the crystal field brought by the dopant itself diminishes the on-site anisotropy of Mn ions and changes both the nature of exchange couplings and spin configuration.<sup>5</sup> Accordingly, the low-temperature freezing processes observed in the pristine material are not effective in these segments and one can justify the two different spin dynamics probed by protons assuming that  $1/T_1^l$  component is measured in Li-depleted chains, while  $1/T_1^s$  in Li-rich chains.

The ratio between the two components estimated from  ${}^1\text{H}$  recovery laws [ $\approx 4$ ; see Eq. (2)] is indeed temperature and field independent, indicating that it quantitatively represents the spatial fraction of the two spin configurations in the material. It is worth pointing out that from high-resolution x-ray diffraction (XRD) there is no evidence of a macroscopic segregation in Li-rich and Li-depleted phases, and therefore they must coexist at the microscopic level. Moreover, XRD line

shape and width indicate the absence of finite-size effects which could arise if very short chain segments were present. This confirms our observation that most of the material is still in the pristine state, where the chain average length is still very long, as one could infer noticing that  $1/T_1^s \propto 1/H^{0.5}$  at high temperature, as expected for extended one-dimensional systems. Hence, most of protons are very far from boundaries. On the other hand, a small fraction of the material is built of Li-rich segments. From our data we can give a lower limit for the average length of Li-rich segments, based on the observation that no peak in  ${}^7\text{Li}$   $1/T_1$  is detected and that its low-temperature value is more than two orders of magnitude smaller than  $1/T_1^s$  (see Figs. 6 and 7). This implies an average dipolar hyperfine coupling of  ${}^7\text{Li}$  nuclei with the Mn spins in Li-depleted segments more than an order of magnitude smaller than the one of protons in the same segments. Taking into account that the dipolar coupling decreases as  $1/r^3$ , one can roughly estimate 12 lattice steps as a lower limit for the length of the Li-rich segments and 4 lattice steps for the separation among adjacent Li-rich chain segments. It is clear that the disorder associated with the presence of alternating Li-rich and Li-depleted regions would perturb the electron delocalization along the chain and cause an activated transport mechanism, as will be discussed in the following.

At high temperature, around 180 K,  ${}^7\text{Li}$   $1/T_1$  shows a broad maximum (Fig. 7). One could argue that this maximum is analogous to the one observed in  $1/T_1^s$  at low temperature and that it could arise from a spin freezing. However, at variance with what is found at  $T \approx 10$  K, no evidence of a spin freezing around 200 K is present in the magnetization data (see Fig. 2). Another mechanism that could give rise to a maximum is Li diffusion, with a hopping frequency reaching the MHz range around 200 K. However, if this was the case  ${}^7\text{Li}$  NMR linewidth should be much narrower and should not follow the same temperature dependence of the macroscopic susceptibility (Fig. 10). Moreover, if Li was diffusing, one should not observe a stretched exponential recovery of nuclear magnetization with a temperature-independent exponent  $\beta$  (Fig. 4). Therefore,  ${}^7\text{Li}$  relaxation has to originate from a different mechanism.

In Li-rich chain segments the electrons should start filling  $2e_g(\pi)$  orbitals, which overlap with the orbitals of adjacent molecules to form a one-dimensional band.<sup>3,11</sup> However, the electron delocalization can be prevented by a strong Coulomb repulsion, as well as by the disorder associated with the nonuniform Li distribution. Accordingly, an effective gap between localized and itinerant states develops. In this scenario one can ascribe to the electron a phenomenological<sup>19</sup> hopping time  $\tau_e = \tau_e^0 \exp(E_g/T)$  with  $\tau_e^0$  renormalized with respect to its bare value  $\tau_e^0 \approx \hbar/W$  ( $W$  the bandwidth) owing to spin-polaron formation and other effects,<sup>20</sup> while  $E_g$  is an effective gap between localized and delocalized states.

The disorder, already evidenced by the stretched exponential recovery, causes a distribution of  $E_g$ 's. If one assumes a rectangular distribution of  $E_g$ 's, one obtains again an expression for  $1/T_1$  as in Eq. (9). It is noticed that for a width of the distribution of the order of its average value (i.e.,  $\langle E_g \rangle \approx \Delta_g$ ), at low temperature  $1/T_1 \propto T$ . Although this temperature de-

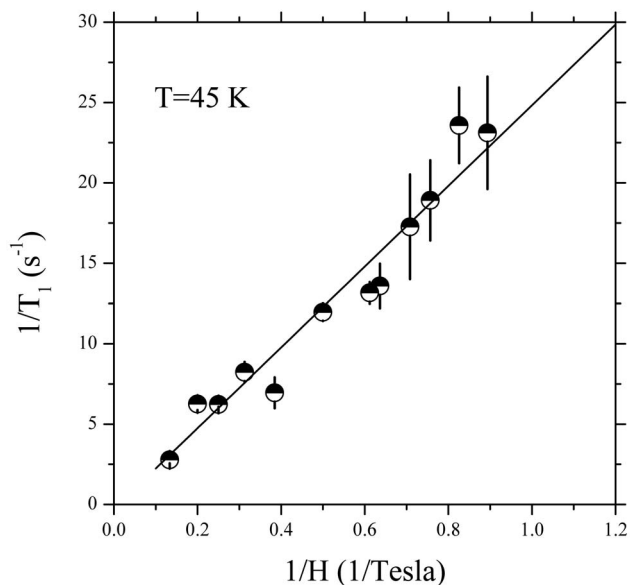


FIG. 11.  ${}^7\text{Li}$  nuclear spin-lattice relaxation rate, at  $T=45$  K, reported as a function of  $1/H$ . The solid line shows the behavior expected from Eq. (9) for  $\langle E_g \rangle = \Delta_g = 410$  K.

pendence is the same one expected for a metal, here it has quite a different origin. Moreover, while in a one-dimensional metal  $1/T_1$  should be either frequency independent or increase as  $1/\sqrt{H}$ ,<sup>21</sup> from Eq. (9),  $1/T_1$  should increase as  $1/\omega_N \propto 1/H$ , as  $T \rightarrow 0$ . We find that the temperature and magnetic field dependence of  $1/T_1$  can be accounted for by Eq. (9) with  $\langle E_g \rangle = \Delta_g = 410 \pm 46$  K and a  $\tau_e^0 = (3 \pm 0.8) \times 10^{-10}$  s (see Figs. 7 and 11). Although it is not easy to give a definite statement in favor of this relaxation mechanism on the basis of our data alone, we point out that this phenomenological model for the electron diffusion along the chain can satisfactorily explain  ${}^7\text{Li}$  NMR data. A homogeneous Li distribution or, in other terms, less disorder would possibly allow one to observe a metallic behavior in  $\text{Li}_x\text{MnPc}$ .

#### IV. CONCLUSIONS

From NMR measurements we have addressed the study of the modifications of the microscopic properties of  $\beta\text{-MnPc}$  upon doping with alkali ions. We have observed that in  $\text{Li}_{0.5}\text{MnPc}$ , two different dynamics coexist at the microscopic level: a first one arising from the freezing of MnPc spins, which is similar to the one observed in the undoped compound and is associated with Li depleted regions, and a second one, characteristic of Li-rich regions, associated with the hopping of the electrons along the chain, whose delocalization is hindered by the disorder and the Coulomb and spin interactions. The temperature dependence of the characteristic correlation time for each one of these two processes was derived and compared to the one obtained from macroscopic techniques. These phthalocyanines could possibly become metallic for Li contents  $x=2$  and  $x=4$ , where  $\text{Li}_x\text{MnPc}$  shows a more homogeneous distribution of Li ions and less disorder is present.<sup>21</sup>

## ACKNOWLEDGMENTS

This work was supported by PRIN2004 National Project

“Strongly Correlated Electron Systems with Competing Interactions” and by Fondazione CARIPLO 2005 Scientific Research funds.

- 
- <sup>1</sup>See, for example, *Applications of Phthalocyanines, Vol. 19 of The Porphyrin Handbook*, edited by K. M. Kadish, K. M. Smith, and R. Guilard (Academic Press, San Diego, 2003); *Phthalocyanines: Properties and Applications*, edited by C. C. Leznoff and A. B. P. Lerner (VCH, New York, 1966), Vol. 4.
- <sup>2</sup>M. F. Craciun, S. Rogge, M. J. L. den Boer, S. Margadonna, K. Prassides, Y. Iwasa, and A. F. Morpurgo, *Adv. Mater. (Weinheim, Ger.)* **18**, 320 (2006).
- <sup>3</sup>E. Tosatti, M. Fabrizio, J. Tóbiš, and G. E. Santoro, *Phys. Rev. Lett.* **93**, 117002 (2004).
- <sup>4</sup>M. Capone, M. Fabrizio, C. Castellani, and E. Tosatti, *Phys. Rev. Lett.* **93**, 047001 (2004).
- <sup>5</sup>Y. Taguchi, T. Miyake, S. Margadonna, K. Kato, K. Prassides, and Y. Iwasa, *J. Am. Chem. Soc.* **128**, 3313 (2006).
- <sup>6</sup>D. Jérôme and H. J. Schulz, *Adv. Phys.* **31**, 299 (1982).
- <sup>7</sup>C. G. Barraclough, R. L. Martin, S. Mitra, and R. C. Sherwood, *J. Chem. Phys.* **53**, 1638 (1970).
- <sup>8</sup>F. Tedoldi, A. Campana, and P. Carretta, *Eur. Phys. J. B* **7**, 219 (1999).
- <sup>9</sup>S. Lee, M. Yudkowsky, W. P. Halperin, M. Y. Ogawa, and B. M. Hoffman, *Phys. Rev. B* **35**, 5003 (1987).
- <sup>10</sup>H. Benner and J. P. Boucher, in *Magnetic Properties of Layered Transition Metal Compounds*, edited by L. J. de Jongh (Kluwer Academic, Dordrecht, 1990), p. 323.
- <sup>11</sup>M. S. Liao and S. Scheiner, *J. Chem. Phys.* **114**, 9780 (2001).
- <sup>12</sup>L. Forro and L. Mihaly, *Rep. Prog. Phys.* **64**, 649 (2001).
- <sup>13</sup>M. Evangelisti, J. Bartolomé, L. J. de Jongh, and G. Filoti, *Phys. Rev. B* **66**, 144410 (2002).
- <sup>14</sup>L. Bogani, A. Caneschi, M. Fedi, D. Gatteschi, M. Massi, M. A. Novak, M. G. Pini, A. Rettori, R. Sessoli, and A. Vindigni, *Phys. Rev. Lett.* **92**, 207204 (2004).
- <sup>15</sup>F. Ferraro, D. Gatteschi, A. Rettori, and M. Corti, *Mol. Phys.* **85**, 1073 (1995).
- <sup>16</sup>A. Lascialfari, Z. H. Jang, F. Borsa, P. Carretta, and D. Gatteschi, *Phys. Rev. Lett.* **81**, 3773 (1998).
- <sup>17</sup>M. Corti, S. Marini, A. Rigamonti, F. Tedoldi, D. Capsoni, and V. Massarotti, *Phys. Rev. B* **56**, 11056 (1997).
- <sup>18</sup>A. Rigamonti, F. Borsa, and P. Carretta, *Rep. Prog. Phys.* **61**, 1367 (1998).
- <sup>19</sup>P. Carretta, M. Corti, and A. Rigamonti, *Phys. Rev. B* **48**, 3433 (1993).
- <sup>20</sup>L. Zuppiroli, M. N. Bussac, S. Paschen, O. Chauvet, and L. Forro, *Phys. Rev. B* **50**, 5196 (1994); M. M. Fogler, S. Teber, and B. I. Shklovskii, *ibid.* **69**, 035413 (2004).
- <sup>21</sup>G. Soda, D. Jérôme, M. Weger, J. M. Fabre, and L. Giral, *Solid State Commun.* **18**, 1417 (1976); P. Carretta, C. Berthier, M. Horvatić, Y. Fagot-Revurat, P. Ségransan, D. Jérôme, and C. Bourbonnais, in *Physical Phenomena at High Magnetic Fields-II*, edited by Z. Fisk, Lev Gorkov, D. Melzer, and R. Schriffer (World Scientific, Singapore, 1996), p. 328.